J. Biochem. 131, 137–143 (2002)

Crystal Structure of the Antigen-Binding Fragment of Apoptosis-Inducing Mouse Anti-Human Fas Monoclonal Antibody HFE7A

Shuichiro Ito,[1] Tomoko Takayama, Hiroyuki Hanzawa, Kimihisa Ichikawa, Jun Ohsumi, Nobufusa Serizawa, Tadashi Hata, and Hideyuki Haruyama

Biomedical Research Laboratories, Sankyo Co., Ltd., 140-8710

Received August 10, 2001; accepted November 13, 2001

Binding of Fas ligand to Fas induces apoptosis. The Fas-Fas ligand system plays important roles in many biological processes, including the elimination of autoreactive lymphoid cells. The mouse anti-human Fas monoclonal antibody HFE7A (m-HFE7A), which induces apoptosis, has been humanized based on a structure predicted by homology modeling. A version of humanized HFE7A is currently under development for the treatment of autoimmune diseases such as rheumatoid arthritis. For a deeper understanding of the protein engineering aspect of antibody humanization, for which information on the three-dimensional structure is essential, we determined the crystal structure of the m-HFE7A antigen-binding fragment (Fab) by X-ray crystallography at 2.5 Å resolution. The main-chain conformation of the five loops in the six complementarity-determining regions (CDRs) was correctly predicted with root-mean-square deviations of 0.30–1.04 Å based on a comparison of the crystal structure with the predicted structure. The CDR-H3 conformation of the crystal structure, which was not classified as one of the canonical structures, was completely different from that of the predicted structure but adopted the conformation which followed the "H3-rules." The results of charge distribution analysis of the antigen-binding site suggest that electrostatic interactions may be important for its binding to Fas.

Key words: agonistic antibody, apoptosis, crystal structure, Fab, Fas.

Apoptosis, or programmed cell death, is involved in many biological processes, including embryogenesis, development of the immune system, elimination of virus-infected cells and maintenance of tissue homeostasis (*1*). Binding of Fas ligand (FasL) or agonistic antibodies to Fas induces apoptosis. Fas is a type-I membrane protein belonging to the tumor necrosis factor (TNF) receptor superfamily (*2, 3*), and FasL is a member of the TNF family (*4*). Mice with mutations of Fas and/or FasL develop massive lymphadenopathy and autoimmune diseases, which indicates that the Fas-FasL system plays an important role in the elimination of autoreactive lymphoid cells (*5, 6*).

The mouse monoclonal antibody HFE7A (m-HFE7A), raised against human Fas, binds to both human and mouse Fas (*7, 8*). The administration of m-HFE7A to mice induces apoptosis in thymocytes. However, in mice, m-HFE7A shows no sign of the hepatotoxicity observed with the hamster anti-murine Fas monoclonal antibody Jo2 (*9*). Moreover, the administration of m-HFE7A to mice prevents the injury to the liver induced by Jo2. Therefore, m-HFE7A may be useful for the treatment of autoimmune diseases such as rheumatoid arthritis and fulminant hepatitis.

Humanization is a procedure required to enable murine antibodies to be used in humans since murine antibodies are immunogenic in humans (*10*). Direct grafting of only the residues in the murine complementarity-determining regions (CDRs) that are mainly involved in the binding with the antigen into human antibodies has sometimes decreased the binding affinity (*11*). Therefore, it is important to graft both the murine CDR residues and a small number of murine residues maintaining the conformation of the CDR residues. m-HFE7A has been humanized using a structure predicted by homology modeling to limit the number of mouse residues as much as possible and to reduce the immunogenicity (*12*). A humanized version of m-HFE7A is currently under development for human therapy.

To further understand antibody humanization and to ultimately elucidate the mechanism of apoptosis induced by agonistic antibodies, we determined the crystal structure of the m-HFE7A Fab by X-ray crystallography at 2.5 Å resolution. Here, we describe comparison of the crystal structure with the predicted structure, with special reference to the main-chain conformation of the CDR residues.

MATERIALS AND METHODS

Protein Purification, Crystallization, and X-Ray Data Collection—The preparation, purification, and crystallization of the m-HFE7A (IgG1, κ light chain) Fab were described previously (*7, 13*). The C-terminal residue of the H

[1] To whom correspondence should be addressed. Phone: +81-3-3492-3131, Fax: +81-3-5436-8565, E-mail: shuici@shina.sankyo.co.jp

Abbreviations: CDR, complementarity-determining-region; CDR-L1, CDR-L2, CDR-L3, CDR-H1, CDR-H2, and CDR-H3, the six CDR loops defined by Kabat *et al.* (*32*); C_L and C_{H1}, constant domains of the light and heavy chains; Fab, antigen-binding fragment; L and H, light and heavy; residues are numbered according to Kabat *et al.* (*32*); rms, root-mean-square; V_L and V_H, variable domains of the light and heavy chains.

TABLE I. **Data collection and refinement statistics.**

Data collection	
Number of crystals used	1
Maximum resolution	2.5
Observed reflections	69,732
Unique reflections	15,256
Completeness (%)	97.8 (97.8)
Average redundancy	4.6
I/sigma	32.3 (10.5)
R_{merge}[a]	0.045 (0.092)
Refinement	
Resolution range	40.0-2.5
Reflections ($F \geq 2\sigma(F)$)	14,984
Completeness (%)	96.2 (95.6)
Number of non-hydrogen atoms	3,444
Number of water molecules	57
R-factor[b]	0.168 (0.211)
Free *R*-factor[c]	0.241 (0.306)

[a] $R_{merge} = \Sigma_{hkl}|I-\langle I\rangle|/\Sigma_{hkl}\langle I\rangle$. [b] *R*-factor = $\Sigma||F_{obs}|-|F_{calc}||/\Sigma|F_{calc}|$. [c] Free *R*-factor (*43*) is calculated for 1,178 reflections (7.9%) excluded from all refinement. Values in parentheses are for the highest resolution shell.

chain in the Fab was determined by mass spectrometry using the ^{18}O-labeling technique (*14*). Briefly, the Fab [10 mg ml^{-1} in 10 mM Tris-HCl (pH 7.4)] was crystallized at 296 K by the hanging drop vapor-diffusion method, with equilibration against the reservoir solution containing 1.2 M sodium citrate, 3% 2-methyl-2,4-pentanediol, and 10 mM sodium borate (pH 8.5). Crystals suitable for X-ray diffraction analysis were grown by means of the streak seeding technique (*15*), with equilibration against 1.2 M sodium citrate and 10 mM sodium borate (pH 8.5). The crystals appeared within a few days and reached maximum dimensions of 0.35 × 0.25 × 0.2 mm^3 in 1 week. The crystals belong to orthorhombic spacegroup $P2_12_12_1$ with unit cell dimensions of a = 43.4 Å, b = 74.0 Å, c = 133.8 Å. The asymmetric unit contains one Fab molecule, with a V_M of 2.2 $Å^3$ Da^{-1} (*16*). Intensity data were collected at room temperature using synchrotron radiation at the BL-6B station (The Photon Factory, Tsukuba) with λ set to 1.0 Å. Diffraction data were processed with programs DENZO and SCALEPACK (*17*).

Phase Determination and Structure Refinement—The structure of the m-HFE7A Fab was determined by molecular replacement using program X-PLOR (*18*). As a search model for the variable domain in molecular replacement, the predicted structure for the humanization of the m-HFE7A antibody was used. The predicted structure was constructed by the combination of programs AbM (Oxford Molecular) and QUANTA/CHARM (Molecular Simulations) (*12*). The C_L-C_{H1} domains of the search model corresponded to the Fab fragment of mouse monoclonal antibody An02 (Protein Data Bank code, 1BAF) (*19*). A set of search models with elbow angles (the angle between the two pseudo 2-fold rotation axes of the variable and constant domains) of 124° to 164°, increased every 10°, was created with X-PLOR. A rotation search, Patterson-correlation coefficient refinement (*20*), and translation search were performed for each search model using data from 15.0 to 4.0 Å resolution. After 50 cycles of rigid-body refinement of the correctly oriented and positioned model, the crystallographic R factor dropped to 0.462 for the data from 15.0 to 3.0 Å resolution. Further structure refinement was carried out by the simulated annealing method followed by positional and individual temperature factor refinement using X-PLOR, and manual rebuilding of the Fab model was performed with program O (*21*). At the end of the refinement, positive electron densities above 3σ were assigned as water molecules and the assignments were examined by visual inspection. At the end of each refinement step, model geometry was monitored with O and program PROCHECK (*22*). Solvent-accessible surface and charge distribution analyses were performed with program GRASP (*23*). Crystal contacts were analyzed with X-PLOR using a distance cutoff of 4.0 Å. The data collection and refinement statistics are shown in Table I.

RESULTS AND DISCUSSION

Quality of the Crystal Structure—The final electron-density map allowed the positioning of most residues with confidence (Fig. 1). The model consists of 436 residues from the Fab fragment (215 residues from the L chain and 221 residues from the H chain) and 57 water molecules. The C-terminal residue of the H chain in the Fab was Cys242H, as determined by mass spectrometry (data not shown) using the ^{18}O-labeling technique (*14*). Since the C-terminal region of both chains shows weak electron density and is disordered, residues 212L–214L and residues 229H–242H were not included in the final model. The electron density corresponding to residues 127H–135H is very weak, indicating that the loop is disordered. These residues of the C_H domain, which are in the loop between two adjacent β-strands and exposed to the solvent, were also disordered in other Fab crystal structures. Analysis using PROCHECK indicated good geometry, 88.3% of the residues lying in the most favored regions of the Ramachandran plot, and 11.4% in the allowed regions, with no residues except Ala51L in the disallowed regions. Ala51L is the second amino acid residue of CDR-L2 and is often found in the same γ-turn as in other Fabs (*24*). The average B-factors are 22.4 $Å^2$ for the main-chain atoms of the protein, 24.4 $Å^2$ for the side-chain atoms, and 26.4 $Å^2$ for the oxygen atoms of the water molecules. The estimated coordinate error determined by the method of Luzatti (*25*) is 0.22 Å. The root-mean-square (rms) deviations of bond lengths and angles from ideal values are 0.005 Å and 1.3°, respectively. Nine residues in the six CDRs are involved in crystal contacts. These residues are 27L, 27dL, and 28L from CDR-L1, 52L from CDR-L2, 31H from CDR-H1, and residues 53L–56L from CDR-H2. Considering the similarity to other Fabs, as described below, the crystal contacts do not significantly affect the main-chain conformation of all six CDRs.

Overall and CDR Structures—The overall structure of the four domains (V_L, V_H, C_L, and C_{H1}) from the m-HFE7A Fab is consistent with all other Fab crystal structures previously reported. The elbow angle of 134.2° is in the range commonly observed. Although there is great variation in the sequence and size of the CDR loops, various studies have shown that five of the six CDR loops usually have one of a small number of main-chain conformations, called canonical structures (*26, 27*). The conformation of a particular canonical structure is determined by the length of the loop and the residues present at key positions. Cluster analysis (*28*) has also been applied to the m-HFE7A CDR loops.

Although the crystal structure of the m-HFE7A Fab was

solved by means of molecular replacement using the predicted structure as a search model, the free *R*-factor calculated for 7.9% of the reflections, which were not used for refinement, dropped to 0.241 after refinement, indicating that the final crystal structure is free of bias from the predicted structure. Therefore, it is possible to compare the crystal structure with the predicted structure and the structures deposited in the Protein Data Bank (PDB). For comparison of the crystal structure with the predicted structure used for the design of humanized HFE7As, the backbone atoms (N, Cα, C, and O) of the CDR loops were superposed and the rms deviations were calculated (Table II). The CDR-L1 conformation of the m-HFE7A Fab is very close to that of the 59.1 Fab (PDB code, 1ACY) (*29*), with an rms deviation of 0.51 Å, and corresponds to the type-15B cluster. The m-HFE7A CDR-L1 does not belong to one of the ordinary canonical structures. Based on the length and sequence, CDR-L2 from m-HFE7A belongs to the type-1 canonical class and the type-7A cluster, and the loop is superposed well with CDR-L2 from the L5Mk16 single-chain Fv (PDB code, 1LMK) (*30*), with an rms deviation of 0.31 Å. The CDR-L3 conformation of the m-HFE7A Fab gives an rms deviation of 0.44 Å from that of the Te33 Fab (PDB code, 1TET) (*31*), and corresponds to the type-1 canonical structure and the type-1 cluster.

Residues 31H–35H were defined according to Kabat *et al.* (*32*) as the first CDR of the H chain based on sequence variation. However, structural studies showed that residues 26H–32H have various conformations (*24*). Residues 26H–32H and 31H–35H give rms deviations of 0.44 and 0.42 Å compared with those of the J539 Fab (PDB code, 2FBJ) (*33*), in which the loop from 26H to 32H belongs to the type-1 canonical structure and the type-10A cluster. The CDR-H2 loop of the m-HFE7A Fab is not classified as the type-2 canonical structure, since Val71H of m-HFE7A is not a key residue according to the ordinary canonical definition. However, Val71 of the H chain is an allowed residue according to the results of cluster analysis (*28*). Residues 50H–66H of m-HFE7A give an rms deviation of 0.65 Å, when superposed with those of the 8F5 Fab (PDB code, 1BBD) (*34*), in which the CDR-H2 conformation adopts the type-2 canonical structure and the type-10A cluster.

The CDR-H3 loop is the most variable loop among the six CDR loops in terms of length, amino acid sequence and structure, and thus was not included in the canonical-structure description. Recently, Shirai *et al.* proposed the "H3-rules" (*35, 36*), which partly govern the CDR-H3 conformation dependence on the sequence. The H3-rules can be applied to two regions: at the base and the β-hairpin region of the CDR-H3 loops. According to the H3-rules, the CDR-H3 loop from m-HFE7A adopts a (2:2) β-hairpin structure with a kinked-base, as deduced from its length and amino acid sequence. The crystal structure revealed that the CDR-H3 loop from m-HFE7A had essentially the same main-chain conformation, with an rms deviation of 0.70 Å for the backbone atoms, as that of the 36–71 Fab (PDB code, 6FAB) (*37*), which is known to have a kinked (2:2) β-hairpin conformation (Fig. 2). In the crystal structures, key residues Arg94H and Asp101H are salt-bridged, and the carbonyl-oxygen atom of Phe100dL and HNε1 of Trp103-H form a hydrogen bond, resulting in the kinked-base structure. Key residues in the loop region are Ser99H and Asn100H, resulting in the (2:2) β-hairpin conformation. Therefore, the H3-rules were found to be helpful for predicting the CDR-H3 conformation of m-HFE7A.

Comparison of the Crystal Structure with the Predicted Structure—The crystal structure and the predicted structure used for the humanization and as a search model for molecular replacement were compared after superposing their backbone atoms (Table II and Fig. 3). The predicted structure of the m-HFE7A Fv was initially modeled with the program AbM, which takes into account the canonical structures based on a target amino acid sequence (*12*). The backbone conformation of the CDR loops, which was automatically assigned by the program to have one of the canonical structures, was therefore correctly predicted, with rms deviations of 0.30 Å for CDR-L2, 0.34 Å for CDR-L3, and 0.42 Å for CDR-H1. The CDR-H2 backbone conformations of the two structures, in which one of the key resi-

Fig. 1. **The final electron-density map of the CDR-H3 loop.** The σA-weighted (*44*) ($2|F_o|-|F_c|$) electron-density map was phased using the final model at 2.5 Å resolution. The map is contoured at 1.0σ, where σ is the standard deviation of the electron-density map. The final model is shown as a stick model.

TABLE II. **Rms deviations (Å) after superposition of the crystal structure and other structures.**

Crystal structure CDR	Predicted structure	*Structures in PDB*	
	Rms deviation	Rms deviation	PDB code
L1	1.04	0.51	1ACY
L2	0.30	0.31	1LMK
L3	0.34	0.44	1TET
H1 (Kabat)[a]	0.42	0.42	2FBJ
H1 (Chotia)[a]	0.40	0.44	2FBJ
H2	0.95	0.65	1BBD
H3	2.48	0.70	6FAB

[a]Residues of CDR-H1 are 31H–35H and 26–32H according to the Kabat (*32*) and Chotia (*24*) definitions, respectively.

dues, Val71H, does not follow the definition of the ordinary canonical structure, are similar with an rms deviation of 0.95 Å, since CDR-H2 was manually assigned to have the type-2 canonical structure in the modeling process. However, a significant difference exists in the dihedral angles of ASP54H (ϕ = –129.8°, φ = 2.9° in the crystal structure; ϕ = –133.28°, φ = –117.6 in the predicted structure). Asp54H is located near Val71H and the side-chain conformation of Val71H in the predicted structure was not correctly predicted, which altered the dihedral angles of ASP54H in the modeling process and resulted in increasing rms deviation. The CDR-L1 loop, which belongs to the type-15B cluster, was modeled using the type-15B CDR-L1 loop of the 59.1 Fab as a template. Thus, the CDR-L1 conformation of the predicted structure is very close to that of the crystal structure. The CDR-L1 residues give a slightly large rms deviation of 1.04 Å. The difference in the CDR-L1 conformation mainly occurs at Ser27aL (ϕ = –53.9°, φ = 131.5° in the crystal structure; ϕ = –99.6°, φ = 178.1° in the predicted structure).

The CDR-H3 loop modeled with AbM had a completely different conformation from that of the crystal structure since the H3-rules were not applied. The H3-rules can predict the backbone conformation of the m-HFE7A CDR-H3 loop based on the amino acid sequence and are therefore considered important.

Binding of m-HFE7A to Fas—Depending on the type of antigen, the shape of the antigen-binding site can be classified as a cavity for small antigens, a concave surface for peptides and loops, and a flat surface for proteins (*38*). Surface representation and charge distribution analyses of the m-HFE7A Fab indicated that the antigen-binding site of m-HFE7A has a concave surface and a large proportion of negative charges (Fig. 4). An ELISA experiment revealed that the epitope peptide of m-HFE7A corresponded to residues 105–114 of Fas (Arg-Thr-Gln-Asn-Thr-Lys-Cys-Arg-Cys-Lys) (*39*), which has a large proportion of positively charged residues. The charge of the antigen-binding site of m-HFE7A is complementary to that of the epitope peptide, suggesting that electrostatic interactions are likely to play an important role in the recognition and binding.

Although the three-dimensional structure of Fas has not been determined yet, the crystal structure of the TNFβ and TNF receptor–1 (TNFR1) complex (*40*) allowed us to predict the corresponding region of the epitope peptide in TNFR1. Furthermore, a model of the m-HFE7A/Fas complex is proposed based on data for the epitope peptide together with the surface shape and the charge distribution of the m-HFE7A Fab crystal structure. The TNFβ/TNFR1 structure shows that the second cystein-rich domain (CDR2) and CDR3 of the TNFR1 form the ligand-binding region for TNFβ (Fig. 5a). The epitope peptide of m-HFE7A

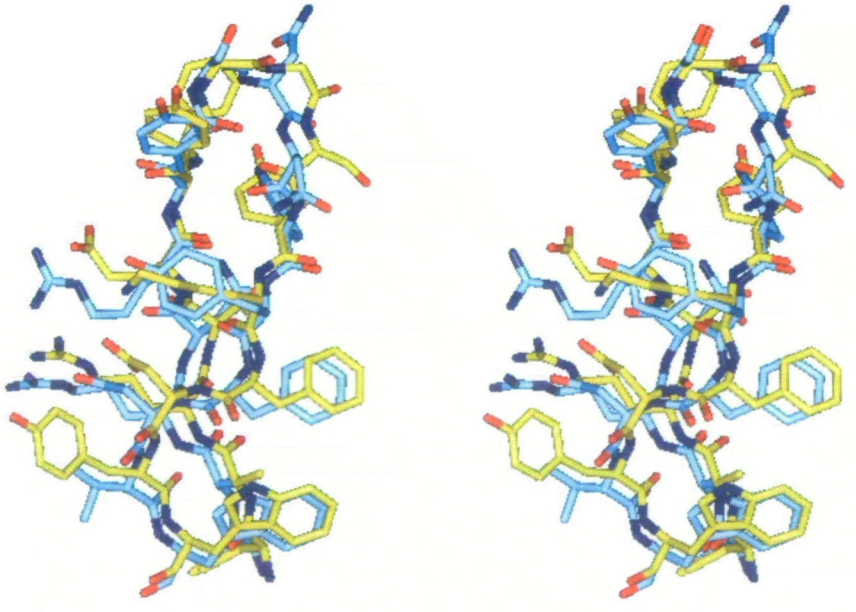

Fig. 2. **Stereoview of the superposition of the CDR-H3 loops from the crystal structures of the m-HFE7A Fab and the 36–71 Fab (*37*).** The figure shows the carbon atoms of the m-HFE7A Fab in cyan, those of the 36–71 Fab in yellow, nitrogen in blue and oxygen in red. Figures 2, 3, and 5 were prepared with Insight II (Molecular Simulations).

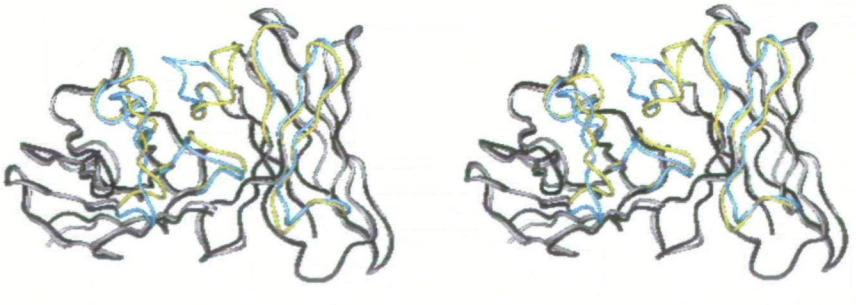

Fig. 3. **Stereoview of the superposition of the two structures: the crystal and predicted structures.** The figure shows the Cα traces for the variable domains. The CDR loops of the crystal and predicted structures are shown in cyan and yellow, respectively. The framework regions of the crystal and predicted structures are shown in black and gray, respectively.

is predicted to form an extended strand in the C-terminal region of CRD2 in Fas. However, m-HFE7A is likely to bind to Fas at a binding site completely different from that of FasL (Fig. 5b).

The first step in signaling by members of the TNFR family was thought to involve ligand-induced trimerization of the receptor. However, recent reports demonstrated that TNFR and Fas in unstimulated cells are constitutively oligomerized before ligand binding through a self-association domain, CDR1, termed the pre-ligand assembly domain, and that the preassembled receptors are nonsignaling (*41, 42*). It is possible that ligand binding induces conformational changes of the oligomerized subunits and/or the formation of oligomers different from that present in the unstimulated state. *In vitro*, m-HFE7A can induce apoptosis only when crosslinked by a second anti-murine antibody, and *in vivo* it is suggested that m-HFE7A is crosslinked by the Fc receptor (*7*). It is also suggested that m-HFE7A might prevent Jo2-induced hepatitis through a mechanism other than simple competition with Jo2 in binding to Fas (*7*). This may be related to the difference in the environment of the target cells; the density of the cells bearing Fc receptors in the liver may be much smaller than that in lymphatic tissues. Currently, the details of the structural mechanism of apoptosis by m-HFE7A remain unclear. Further studies, including determination of the Fas-FasL and Fas-m-HFE7A complex, will help us to understand the mechanism of apoptosis by agonistic antibodies.

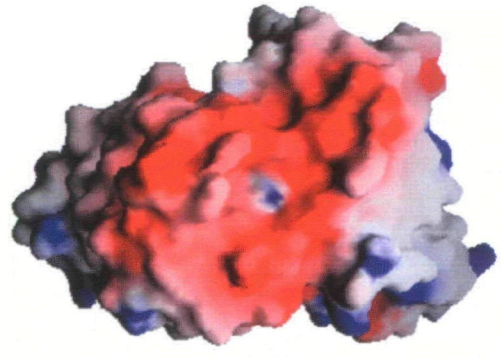

(a)

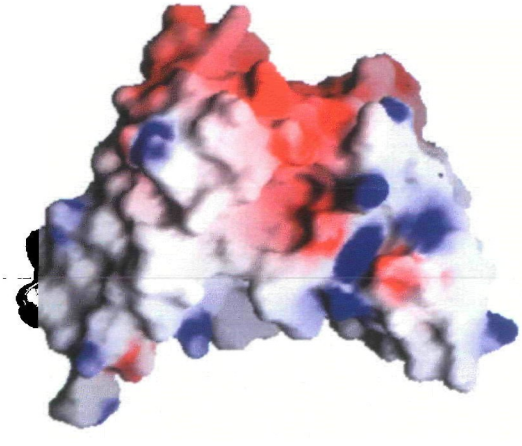

(b)

Fig. 4. **The shape and charge distribution of the m-HFE7A antigen-binding site.** The variable domains are shown. Blue denotes positive charges and red negative charges. The electrostatic potential is contoured at ±10.0 kT with GRASP (*23*). (a) A top view of the antigen binding site. The structure orientation is similar to that in Fig. 3. (b) A side view of the antigen binding site.

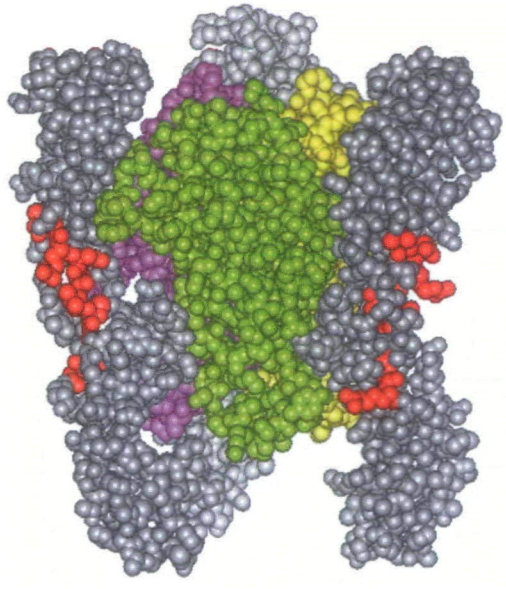

(a)

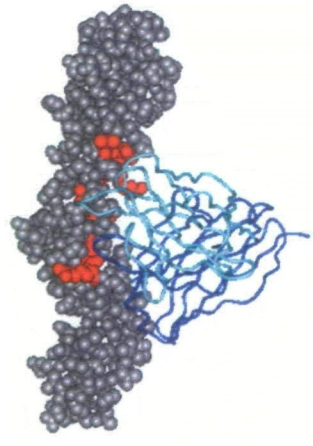

(b)

Fig. 5. **Schematic representation of the proposed complex model for m-HFE7A and its receptor.** (a) The crystal structure of the TNFβ and TNF receptor–1 complex (*40*) is shown. Each TNFβ monomer is shown as a space-filling model in a different color, green, magenta, or yellow. The extracellular domains of TNF receptor–1 are shown as space-filling models colored in gray. The loop corresponding to the epitope peptide of m-HFE7A is colored in red. (b) The proposed model for the m-HFE7A and Fas complex. Only the variable domains of m-HFE7A are shown as Cα traces. The L chain is colored in cyan and the H chain in blue. The crystal structure of TNF receptor–1 was used to represent the extracellular domain of the receptor since the three-dimensional structure of Fas has not been determined yet.

We wish to thank Prof. N. Sakabe of the Structural Biology Sakabe Project (SBSP) of the Foundation for Advanced of International Science (FAIS), and Drs. N. Watanabe, M. Suzuki, and N. Igarashi of the High Energy Accelerator Research Organization for their help in data collection at the Photon Factory. We also thank Y. Matsui for her assistance during the X-ray data collection and figure preparation. S.I. and T.H. are members of SBSP of FAIS. The atomic coordinates and structure factors (code 1IQW) have been deposited in the Protein Data Bank, Research Collaboratory for Structural Bioinformatics, Rutgers University, New Brunswick, NJ.

REFERENCES

1. Nagata, S. (1997) Apoptosis by death factor. *Cell* **88**, 355–365
2. Yonehara, S., Ishii, A., and Yonehara, M. (1989) A cell-killing monoclonal antibody (anti-Fas) to a cell surface antigen co-downregulated with the receptor of tumor necrosis factor. *J. Exp. Med.* **169**, 1747–1756
3. Itoh, N., Yonehara, S., Ishii, A., Yonehara, M., Mizushima, S., Sameshima, M., Hase, A., Seto, Y., and Nagata, S. (1991) The polypeptide encoded by the cDNA for human cell surface antigen Fas can mediate apoptosis. *Cell* **66**, 233–243
4. Suda, T., Takahashi, T., Golstein, P., and Nagata, S. (1993) Molecular cloning and expression of the Fas ligand, a novel member of the tumor necrosis factor family. *Cell* **75**, 1169–1178
5. Watanabe-Fukunaga, R., Brannan, C.I., Copeland, N.G., Jenkins, N.A., and Nagata, S. (1992) Lymphoproliferation disorder in mice explained by defects in Fas antigen that mediates apoptosis. *Nature* **356**, 314–317
6. Takahashi, T., Tanaka, M., Brannan, C.I., Jenkins, N.A., Copeland, N.G., Suda, T., and Nagata, S. (1994) Generalized lymphoproliferative disease in mice, caused by a point mutation in the Fas ligand. *Cell* **76**, 969-976
7. Ichikawa, K., Yoshida-Kato, H., Ohtsuki, M., Ohsumi, J., Yamaguchi, J., Takahashi, S., Tani, Y., Watanabe, M., Shiraishi, A., Nishioka, K., Yonehara, S., and Serizawa, N. (2000) A novel murine anti-human Fas mAb which mitigates lymphadenopathy without hepatotoxicity. *Int. Immunol.* **12**, 555–562
8. Yoshida-Kato, H., Ichikawa, K., Yamaguchi, J., Watanabe, K., Ohsumi, J., Yonehara, S., and Serizawa, N. (2000) Cloning and expression of a novel murine anti-human Fas antibody. *Biosci. Biotechnol. Biochem.* **64**, 1903–1908
9. Ogasawara, J., Watanabe-Fukunaga, R., Adachi, M., Matsuzawa, A., Kasugai, T., Kitamura, Y., Itoh, N., Suda, T., and Nagata, S. (1993) Lethal effect of the anti-Fas antibody in mice. *Nature* **364**, 806–809
10. Queen, C., Schneider, W.P., Selick, H.E., Payne, P.W., Landolfi, N.F., Duncan, J.F., Avdalovic, N.M., Levitt, M., Junghans, R.P., and Waldmann, T.A. (1989) A humanized antibody that binds to the interleukin 2 receptor. *Proc. Natl. Acad. Sci. USA* **86**, 10029–10033
11. Jones, P.T., Dear, P.H., Foote, J., Neuberger, M.S., and Winter, G. (1986) Replacing the complementarity-determining regions in a human antibody with those from a mouse. *Nature* **321**, 522–525
12. Serizawa, N., Haruyama, H., Nakahara, K., and Tamaki, I. (2000) Humanized anti-Fas antibody. Japan Kokai Tokkyo Koho, 2000-166574
13. Ito, S., Takayama, T., Hanzawa, H., Ichikawa, K., Ohsumi, J., Serizawa, N., Haruyama, H., and Hata, T. (2001) Crystallization and preliminary X-ray crystallographic studies on an Fab fragment of the mouse anti-human Fas monoclonal antibody HFE7A. *Acta Cryst.* **D57**, 1700–1702
14. Kosaka, T., Takazawa, T., and Nakamura, T. (2000) Identification and C-terminal characterization of proteins from two-dimensional polyacrylamide gels by a combination of isotopic labeling and nanoelectrospray Fourier transform ion cyclotron resonance mass spectrometry. *Anal. Chem.* **72**, 1179–1185
15. Stura, E.A. and Wilson, I.A. (1991) Application of the streak seeding technique in protein crystallization. *J. Cryst. Growth* **110**, 270–282
16. Matthews, B.W. (1968) Solvent content of protein crystals. *J. Mol. Biol.* **33**, 491–497
17. Otwiniski, Z. and Minor, W. (1997) Processing X-ray diffraction data collected in oscillation mode in *Methods in Enzymology* (Carter, C.W., Jr. and Sweet, R.M., eds.) Vol. 276, pp. 307–326, Academic Press, New York
18. Brünger, A.T. (1993) *X-PLOR 3.1: A System for X-Ray Crystallography and NMR*, Yale University Press, New Haven and London
19. Brünger, A.T., Leahy, D.J., Hynes, T.R., and Fox, R.O. (1991) 2.9 Å resolution structure of an anti-dinitrophenyl-spin-label monoclonal antibody Fab fragment with bound hapten. *J. Mol. Biol.* **221**, 239–256
20. Brünger, A.T. (1990) Extension of molecular replacement: A new search strategy based on Patterson correlation refinement. *Acta Cryst.* **A46**, 46–57
21. Jones, T.A., Zou, J.-Y., Cowan, S.W., and Kjeldgaard, M. (1991) Improved methods for building protein models in electron density maps and the location errors in these models. *Acta Cryst.* **A47**, 110–119
22. Laskowski, R.A., MacArthur, M.W., Moss, D.S., and Thornton, J.M. (1993) PROCHECK: a program to check the stereochemical quality of protein structures. *J. Appl. Crystallog.* **26**, 283–291
23. Nicholls, A., Sharp, K.A., and Honig, B. (1991) Protein folding and association: insights from the interfacial and thermodynamic properties of hydrocarbons. *Proteins* **11**, 281–296
24. Al-Lazikani, B., Lesk, A.M., and Chothia, C. (1997) Standard conformations for the canonical structures of immunoglobulins. *J. Mol. Biol.* **273**, 927–948
25. Luzatti, V. (1952) Traitement statistique des erreurs dans la determination des structures cristallines. *Acta Cryst.* **A5**, 802–810
26. Chothia, C. and Lesk, A.M. (1987) Canonical structures for the hypervariable regions of immunoglobulins. *J. Mol. Biol.* **196**, 901–917
27. Chothia, C., Lesk, A.M., Tramontano, A., Levitt, M., Smith-Gill, S.J., Air, G., Sheriff, S., Padlan, E.A., Davies, D., and Tulip, W.R. (1989) Conformations of immunoglobulin hypervariable regions. *Nature* **342**, 877–883
28. Martin, A.C. and Thornton, J.M. (1996) Structural families in loops of homologous proteins: automatic classification, modelling and application to antibodies. *J. Mol. Biol.* **263**, 800–815
29. Ghiara, J.B., Stura, E.A., Stanfield, R.L., Profy, A.T., and Wilson, I.A. (1994) Crystal structure of the principal neutralization site of HIV-1. *Science* **264**, 82–85
30. Perisic, O., Webb, P.A., Holliger, P., Winter, G., and Williams, R.L. (1994) Crystal structure of a diabody, a bivalent antibody fragment. *Structure* **2**, 1217–1226
31. Shoham, M. (1993) Crystal structure of an anticholera toxin peptide complex at 2.3 Å. *J. Mol. Biol.* **232**, 1169–1175
32. Kabat, E.A., Wu, T.T., Perry, H.M., Gottesman, K.S., and Foeller, C. (1991) *Sequences of Proteins of Immunological Interest*, NIH, Bethesda, MD
33. Suh, S.W., Bhat, T.N., Navia, M.A., Cohen, G.H., Rao, D.N., Rudikoff, S., and Davies, D.R. (1986) The galactan-binding immunoglobulin Fab J539: an X-ray diffraction study at 2.6-Å resolution. *Proteins* **1**, 74–80
34. Tormo, J., Stadler, E., Skern, T., Auer, H., Kanzler, O., Betzel, C., Blaas, D., and Fita, I. (1992) Three-dimensional structure of the Fab fragment of a neutralizing antibody to human rhinovirus serotype 2. *Protein Sci.* **1**, 1154–1161
35. Shirai, H., Kidera, A., and Nakamura, H. (1996) Structural classification of CDR-H3 in antibodies. *FEBS Lett.* **399**, 1–8
36. Shirai, H., Kidera, A., and Nakamura, H. (1999) H3-rules: identification of CDR-H3 structures in antibodies. *FEBS Lett.* **455**, 188–197
37. Strong, R.K., Campbell, R., Rose, D.R., Petsko, G.A., Sharon, J., and Margolies, M.N. (1991) Three-dimensional structure of murine anti-p-azophenylarsonate Fab 36-71. 1. X-ray crystallography, site-directed mutagenesis, and modeling of the complex with hapten. *Biochemistry* **30**, 3739–3748

38. MacCallum, R.M., Martin, A.C., and Thornton, J.M. (1996) Antibody-antigen interactions: contact analysis and binding site topography. *J. Mol. Biol.* **262**, 732–745
39. Serizawa, N., Haruyama, H., Takahashi, T., Yoshida-Kato, H., Ichikawa, K., Ohsumi, J., Ohtsuki, M., Shiraishi, A., and Yonehara, S. (1999) Anti-Fas antibody. Japan Kokai Tokkyo Koho, H11-171900
40. Banner, D.W., DArcy, A., Janes, W., Gentz, R., Schoenfeld, H.J., Broger, C., Loetscher, H., and Lesslauer, W. (1993) Crystal structure of the soluble human 55 kd TNF receptor–human TNF beta complex: implications for TNF receptor activation. *Cell* **73**, 431–445
41. Chan, F.K., Chun, H.J., Zheng, L., Siegel, R.M., Bui, K.L., and Lenardo, M.J. (2000) A domain in TNF receptors that mediates ligand-independent receptor assembly and signaling. *Science* **288**, 2351–2354
42. Siegel, R.M., Frederiksen, J.K., Zacharias, D.A., Chan, F.K., Johnson, M., Lynch, D., Tsien, R.Y., and Lenardo, M.J. (2000) Fas preassociation required for apoptosis signaling and dominant inhibition by pathogenic mutations. *Science* **288**, 2354–2357
43. Brünger, A.T. (1992) Free R value: a novel statistical quantity for assessing the accuracy of crystal structures. *Nature* **355**, 472–475
44. Read, R.J. (1986) Improved Fourier coefficients for maps using phases from partial structures with errors. *Acta Cryst.* **A42**, 140–149